

# CONSTRAINT ON ADDITIONAL PLANETS IN PLANETARY SYSTEMS DISCOVERED THROUGH THE CHANNEL OF HIGH-MAGNIFICATION GRAVITATIONAL MICROLENSING EVENTS

I.-G. SHIN, C. HAN<sup>†</sup>, J.-Y. CHOI, K.-H. HWANG, Y. K. JUNG, H. PARK

Department of Physics, Institute for Astrophysics, Chungbuk National University, Cheongju 371-763, Republic of Korea

<sup>†</sup>Corresponding author

*Draft version December 19, 2021*

## ABSTRACT

High-magnification gravitational microlensing events provide an important channel of detecting planetary systems with multiple giants located at their birth places. In order to investigate the potential existence of additional planets, we reanalyze the light curves of the eight high-magnification microlensing events for each of which a single planet was previously detected. The analyzed events include OGLE-2005-BLG-071, OGLE-2005-BLG-169, MOA-2007-BLG-400, MOA-2008-BLG-310, MOA-2009-BLG-319, MOA-2009-BLG-387, MOA-2010-BLG-477, and MOA-2011-BLG-293. We find that including an additional planet improves fits with  $\Delta\chi^2 < 80$  for seven out of eight analyzed events. For MOA-2009-BLG-319, the improvement is relatively big with  $\Delta\chi^2 \sim 143$ . From inspection of the fits, we find that the improvement of the fits is attributed to systematics in data. Although no clear evidence of additional planets is found, it is still possible to constrain the existence of additional planets in the parameter space. For this purpose, we construct exclusion diagrams showing the confidence levels excluding the existence of an additional planet as a function of its separation and mass ratio. We also present the exclusion ranges of additional planets with 90% confidence level for Jupiter, Saturn, and Uranus-mass planets.

*Subject headings:* gravitational lensing: micro – planetary systems

## 1. INTRODUCTION

Since the first discoveries (Wolszczan & Frail 1992; Mayor & Queloz 1995), the number of known extra-solar planets has been rapidly increasing and it reaches  $\sim 2000$  (<http://exoplanet.eu>: Schneider et al. 2011). A significant fraction of these planets are members of multi-planet systems (Rowe et al. 2014; Lissauer et al. 2012), which were mostly discovered by the radial-velocity and transit methods.

Multi-planet systems can also be detected by using the microlensing method. Gravitational microlensing occurs by the chance alignment along the line of sight toward a background star (source) and a foreground object (lens), resulting in the magnification of the source brightness due to the bending of light by the gravity of the lens. When a lensing object is a star accompanied by a planet, the planet causes astigmatism in the bending of light and induces formation of caustics which refers to the envelope of light rays on the source plane at which the magnification of a point source becomes infinity. A planetary lensing signal occurs when the source approaches caustics and it appears as a short term anomaly superposed on the smooth and symmetric lensing light curve of the host star (Mao & Paczyński 1991; Gould & Loeb 1992). If a planetary system is composed of multiple planets, each planet induces its own caustics and the multiplicity of the planets can be identified if the source trajectory passes multiple caustics induced by the individual planets (Han et al. 2001; Han 2005). The sensitivity to multiple planets for general microlensing events is low because planet-induced caustics are small and thus the geometrical probability for the source to pass multiple caustics is low. However, the sensitivity is high for a subset of lensing events where the brightness of a source star is greatly magnified (Gaudi et al. 1998). This is because one of the caustics induced by each planet is always located very close to the host star around which the source of a high-magnification event passes by (Griest & Safizadeh

1998). Indeed, two multi-planet systems identified by microlensing (Gaudi et al. 2008; Han et al. 2013) were discovered through this channel.

Microlensing discoveries of multi-planet systems are important for better understanding of planet-formation mechanism. According to the core accretion theory (Ida & Lin 2004), giant planets are believed to form in group in the region beyond the snow line where the lower temperature in this region makes many more solid grains available for accretion into planetesimals. However, most known planets in multiple systems reside well within the snow line. These close-in planets are believed to have migrated from the outer region where they were formed (D’Angelo & Lubow 2008; Lubow & Ida 2011). Detecting planets at their birth places by using the transit and the radial-velocity methods is difficult due to their low sensitivity to wide-separation planets. By contrast, microlensing is sensitive to planets located around and beyond the snow line and thus provides a channel to study planets where they formed.

In this work, we reanalyze the light curves of the eight high-magnification microlensing events for each of which a single planet was previously detected. From the analyses, we investigate the existence of additional planets.

## 2. SAMPLE

In published articles, there exist 29 planetary microlensing events from which 31 planets were found. Among them, events for our analyses are selected based on the following criterion. First, we choose planetary events with high magnifications due to their high sensitivity to multiple planets. With an adopted threshold magnification  $A_{\text{th}} \sim 50$ , there exist 15 events. Among the planetary systems found from these events, two are already known to be in multi-

TABLE 1  
LIST OF SAMPLE EVENTS AND THE PROPERTIES OF THE PREVIOUSLY DISCOVERED PLANETS

Event	$A_{\max}$	Previously discovered planet Mass	Separation (AU)	Reference
OGLE-2005-BLG-071	59	$3.8^{+0.4}_{-0.4} M_J$	$3.6^{+0.2}_{-0.2}$	Udalski et al. (2005), Dong et al. (2009)
OGLE-2005-BLG-169	880	$13^{+6}_{-8} M_{\oplus}$	$2.7^{+1.7}_{-1.4}$	Gould et al. (2006)
MOA-2007-BLG-400	629	$0.83^{+0.49}_{-0.31} M_J$	$0.72^{+0.38}_{-0.16} / 6.5^{+3.2}_{-1.2}$	Dong et al. (2009)
MOA-2008-BLG-310	366	$74^{+17}_{-17} M_{\oplus}$	$1.25^{+0.10}_{-0.10}$	Janczak et al. (2010)
MOA-2009-BLG-319	208	$50^{+44}_{-24} M_{\oplus}$	$2.4^{+1.2}_{-0.6}$	Miyake et al. (2011)
MOA-2009-BLG-387	49	$2.6^{+4.1}_{-1.6} M_J$	$1.8^{+0.9}_{-0.7}$	Batista et al. (2011)
MOA-2010-BLG-477	599	$1.5^{+0.8}_{-0.3} M_J$	$2.0^{+3.0}_{-1.0}$	Bachelet et al. (2012)
MOA-2011-BLG-293	418	$2.4^{+1.5}_{-0.9} M_J$	$1.0^{+0.1}_{-0.1} / 3.4^{+0.4}_{-0.4}$	Yee et al. (2012)

planet systems<sup>†</sup> and another two are in stellar binary systems.<sup>‡</sup> We exclude the events with already-known multi-planet systems and circum-stellar binary planets from our analysis. Second, we choose events with good coverage of the peak region. This is because signatures of multiple planets for high-magnification events show up near the peak of a light curve and thus good coverage of the peak region is essential to constrain additional planets. Third, we confine analysis to events for which there is no ambiguity in the interpretation of the known planetary signals. Applying these criteria leave 8 events including OGLE-2005-BLG-071, OGLE-2005-BLG-169, MOA-2007-BLG-400, MOA-2008-BLG-310, MOA-2009-BLG-387, MOA-2010-BLG-477, and MOA-2011-BLG-293.

In Table 1, we list the lensing events that we analyzed. Also presented are the peak magnifications  $A_{\max}$  of the individual events, the physical parameters (mass and separation from the host) of the previously discovered planets, and the references of the original analyses. In Figure 1, we present the light curves of the events. We note that the same data sets as those used in the original analysis are used in our analysis for the consistency of results.

### 3. ANALYSIS METHOD

In order to investigate the existence of an additional planet for a lensing event with an already known planet, it is required to conduct triple-lens modeling. For a triple-lens system, the image positions for given locations of the lens and source are found by solving the equation of lens mapping (lens equation) that is expressed as

$$\zeta = z - \sum_{k=1}^3 \frac{\epsilon_k}{\bar{z} - \bar{z}_{L,k}}. \quad (1)$$

Here  $k=1, 2$ , and  $3$  denote the individual lens components,  $\zeta = \zeta + i\eta$ ,  $z_{L,k} = x_{L,k} + iy_{L,k}$  and  $z = x + iy$  are the complex notations of the source, lens, and image positions, respectively,

<sup>†</sup> The first known multiple microlensing planetary system is OGLE-2006-BLG-109L, where a host star with a mass  $\sim 0.5 M_{\odot}$  is orbited by two planets with masses  $\sim 0.71 M_J$  and  $\sim 0.27 M_J$  and separations from the host  $\sim 2.3$  AU and  $\sim 4.6$  AU, respectively (Gaudi et al. 2008; Bennett et al. 2010). The second system is OGLE-2012-BLG-0026L, where a host star with a mass  $\sim 0.82 M_{\odot}$  is orbited by two planets with masses  $\sim 0.11 M_J$  and  $\sim 0.67 M_J$  and separations  $\sim 3.8$  AU and  $\sim 4.6$  AU, respectively (Han et al. 2013).

<sup>‡</sup> OGLE-2013-BLG-0341Lb is the first microlensing planet in a binary stellar system, where a terrestrial planet ( $\sim 2 M_{\oplus}$ ) lies at  $\sim 0.8$  AU from its host with a mass  $\sim 0.10$ – $0.15 M_{\odot}$  and the host itself orbits another star with a mass  $\sim 0.15 M_{\odot}$  and a separation  $\sim 10$ – $15$  AU (Gould et al. 2014). The second microlensing planet in binary is OGLE-2008-BLG-092Lb, where a  $\sim 4 M_{\oplus}$  planet orbits a  $\sim 0.7 M_{\odot}$  star at  $\sim 18$  AU. The host has a low-mass companion with  $\sim 0.15 M_{\odot}$  (Poleski et al. 2014).

$\bar{z}$  denotes the complex conjugate of  $z$ , and  $\epsilon_k = M_k/M_{\text{tot}}$  is the mass fraction of each lens component (Witt 1990). Once the image locations are found, the lensing magnification is computed by

$$A = \sum A_i; \quad A_i = \left| \left( 1 - \frac{\partial \zeta}{\partial \bar{z}} \frac{\partial \bar{\zeta}}{\partial z} \right)^{-1} \right|_{z=z_i}, \quad (2)$$

where  $A_i$  is the magnification of each image.

Due to non-linearity, the lens equation for a triple lens system cannot be analytically solved. However, lensing magnifications can be numerically computed by using the method known as the inverse ray-shooting method (Kayser et al. 1986; Schneider & Weiss 1986). In this method, a large number of rays are uniformly shot from the image plane, bent by the lens equation, and land on the source plane. Then, lensing magnifications are computed as the ratio of the number density of rays on the source plane to that on the image plane. The lens equation can also be solved semi-analytically because the equation is expressed as a tenth-order polynomial in  $z$  and the image positions and subsequent lensing magnifications are computed by solving the polynomial (Rhie 2002; Song et al. 2014). The semi-analytic method has an advantage of fast computation but it is difficult to be used for computing lensing magnifications affected by finite-source effects. On the other hand, the numerical method can be used to compute finite-source magnifications but computation is slow.

Describing the light curve of a triple-lensing event requires ten basic parameters. The first three of these parameters describe how the source approaches the lens. They are the time of the closest source approach to a reference position of the lens system,  $t_0$ , the normalized projected separation between the source and the lens reference position at that moment,  $u_0$ , and the Einstein time scale,  $t_E$ , that is defined as the time required for the source to cross the angular Einstein radius of the lens  $\theta_E$ . Another six parameters characterize the lens system. They are the projected separations between the host and the individual planet companions,  $s_1$  and  $s_2$ , and the mass ratios of the companions to the host,  $q_1$  and  $q_2$ , the angle between the source trajectory and the axis connecting the host and the first planet,  $\alpha$ , and the orientation angle of the second planet with respect to the host-first planet axis,  $\psi$ . We note that length scales describing lensing phenomenon are usually expressed in units of  $\theta_E$  and  $u_0$ ,  $s_1$  and  $s_2$  are normalized by  $\theta_E$ . The last parameter is the angular size of the source  $\theta_*$  in unit of the Einstein radius,  $\rho_* = \theta_*/\theta_E$  (normalized source radius). This parameter is needed to describe light curve deviations affected by finite-source effects.

Besides the basic lensing parameters, precise description of lensing light curves often requires additional parameters to

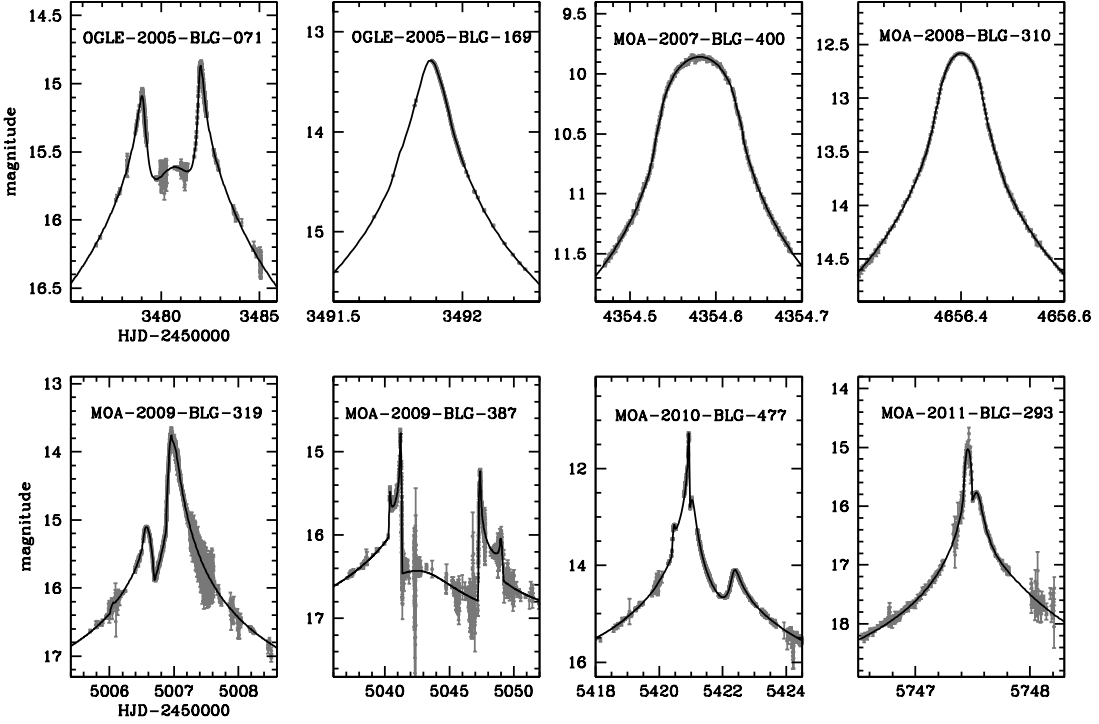


FIG. 1.— Light curves of planetary microlensing events reanalyzed in this work. Grey points with error bars are the data used in our analysis. Also presented are the model light curves base on single-planet models.

account for higher-order effects. One such effect is caused by the positional change of an observer induced by the orbital motion of the Earth around the Sun. Considering this parallax effect (Gould 1992) requires two additional parameters  $\pi_{E,N}$  and  $\pi_{E,E}$  that represent the two components of the lens parallax vector  $\pi_E$  projected on the sky in the north and east equatorial coordinates, respectively. Similarly, lensing light curves can also be affected by the change of the lens position caused by the orbital motion (Shin et al. 2011, 2012; Skowron et al. 2011; Park et al. 2011).

With the lensing parameters, we conduct triple-lens modeling of the events that were previously analyzed based on binary-lens modeling. For all analyzed events, the anomaly is dominated by the signal of the already reported planet and thus the signal of the potential additional planet would be small. We, therefore, set the lensing parameters related to the known planet ( $s_1, q_1$ ) fixed as outlined in Kubas et al. (2008). The existence of an additional planet is then inspected by checking whether the two-planet model improves the fit with respect to the single-planet model. Not knowing the characteristics of the second planet, we search for the second-planet parameters  $s_2$  and  $q_2$  by inspecting solutions in wide ranges of the parameter space spanning  $-1 \leq \log s_2 \leq 1$  and  $-6 \leq \log q_2 \leq 2$ , respectively. For a given set of ( $s_2, q_2$ ), the other lensing parameters are searched for by minimizing  $\chi^2$  in the parameter space using Markov Chain Monte Carlo (MCMC) algorithm.

For computing triple-lensing magnifications, we apply both the semi-analytic and numerical methods. For the region near the peak of the light curve, we use the numerical inverse ray-shooting method because this region is likely to be affected by finite-source effects during the source star’s approach close to the planet-induced caustics. For other regions, we use the semi-analytic method for fast computation. Computing finite-source magnifications is further accelerated by applying the

“map making” method (Dong et al. 2006). In this method, a map of rays for a given set of ( $s_1, q_1$ ) and ( $s_2, q_2$ ) is constructed based on the inverse ray shooting method and then it is used to produce many different light curves resulting from various source trajectories without producing extra maps. In computing finite-source magnifications, we consider limb-darkening variation of the source star surface brightness by modeling the surface brightness profile as  $S_\lambda \propto 1 - \Gamma_\lambda(1 - 1.5 \cos \phi)$ , where  $\Gamma_\lambda$  is the limb-darkening coefficients corresponding to specific passband  $\lambda$  and  $\phi$  is the angle between the line of sight toward the source star and the normal to the source surface. We use the same limb-darkening coefficients that were used in the previous analyses where first planets were reported.

If higher-order effects were reported in the previous analyses, we also consider them. Parallax effects were reported for events OGLE-2005-BLG-071, MOA-2009-BLG-387, and MOA-2010-BLG-477. On the other hand, obvious effect of lens-orbital motion was reported for none of the events. We note that the effect of an additional planet is confined to the narrow region of the light curve peak while both parallax and lens-orbital effects influence the overall shape of a lensing light curve. Therefore, the existence of the second planet does not affect the lensing parameters of higher-order effects.

#### 4. RESULT

##### 4.1. Existence of Additional Planets

Table 2 shows the result of the analysis presented as  $\chi^2$  values of the binary and triple lens models. From the comparison of the  $\chi^2$  values, it is found that including an additional planet improves fits with  $\Delta\chi^2 < 80$  for seven out of the eight analyzed events. For MOA-2009-BLG-319, the improvement is relatively big with  $\Delta\chi^2 = 142.7$ .

Although the improvement of the fit for the event MOA-2009-BLG-319 is formally significant, one cannot exclude the possibility of systematics in data, which is often masqueraded

TABLE 2  
COMPARISON OF BINARY AND TRIPLE LENS FITS AND EXCLUSION RANGE OF A SECOND PLANET

Event	$\chi^2_{\text{bi}}$	$\chi^2_{\text{tri}}$	$\Delta\chi^2$	Exclusion range (AU)		
				Jupiter	Saturn	Uranus
OGLE-2005-BLG-071	1305.6	1283.7	21.9	1.5 – 5.1	–	–
OGLE-2005-BLG-169	533.4	518.5	14.9	0.6 – 11.3	1.0 – 7.1	–
MOA-2007-BLG-400	770.8	760.0	10.8	0.8 – 4.5	1.2 – 2.6	–
MOA-2008-BLG-310	3154.4	3076.4	78.0	0.7 – 2.0	1.1 – 1.3	–
MOA-2009-BLG-319	6180.2	6037.5	142.7	0.5 – 7.9	0.9 – 5.0	1.6 – 2.9
MOA-2009-BLG-387	1298.4	1269.3	29.1	0.9 – 4.4	1.6 – 2.5	–
MOA-2010-BLG-477	4444.0	4394.4	49.6	0.8 – 12.1	1.7 – 5.8	–
MOA-2011-BLG-293	5089.2	5069.9	19.3	1.0 – 3.5	–	–

NOTE. — The  $\chi^2$  difference represents  $\Delta\chi^2 = \chi^2_{\text{bi}} - \chi^2_{\text{tri}}$ , where  $\chi^2_{\text{bi}}$  and  $\chi^2_{\text{tri}}$  are for the binary and triple lens models, respectively. The exclusion ranges are estimated based on 90% confidence level

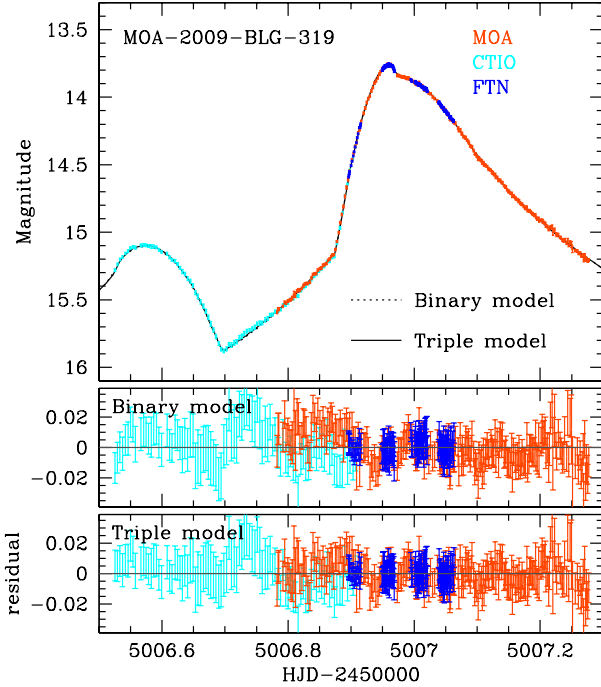


FIG. 2.— Comparison of the triple and binary models of MOA-2009-BLG-319. The lower two panels show the residuals from the individual models.

as planetary signals. In order to check the genuineness of the additional planetary signal, we inspect the fits from the triple and binary lens models. Figure 2 shows the peak portion of the light curve. We plot data sets from MOA, CTIO, and FTN observations for which most signal of the additional planet comes from:  $\Delta\chi^2 = 78.4$  for MOA,  $\Delta\chi^2 = 11.0$  for CTIO, and  $\Delta\chi^2 = 35.5$  for FTN data. Also plotted are the light curves of the triple and binary models. It is found that the two models cannot be distinguished within the resolution of the plot. To better show the difference between the two models, we also present the residuals from the individual models. We find that the improvement by the triple-lens fit is  $\sim 0.01$  mag level which is equivalent to the scatter of the data, implying that the signal can certainly be attributed to the systematics in data. We find similar results for other events. Therefore, we conclude that there is no case of firm detection of additional planets.

#### 4.2. Constraints on Additional Planets

Although no clear evidence of additional planets is found, it is still possible to constrain the existence of additional planets around the lens. The constraint is expected to be strong because all analyzed events are highly magnified and thus efficiency to planets would be high in wide ranges of planet parameters.

For the purpose of constraining additional planets, we construct *exclusion diagrams* (Gaudi & Sackett 2000; Albrow et al. 2000; Kubas et al. 2008; Gould et al. 2010; Cassan et al. 2012) showing the confidence levels excluding the existence of an additional planet as a function of its separation and mass ratio. To construct exclusion diagrams, we first estimate the detection efficiency of planets with respect to the planet parameters  $s_2$  and  $q_2$  according to the following procedure.

- (1) We first choose a triple-lens configuration with  $(s_2, q_2, \psi)$ . For a given set of these parameters, we determine the remaining parameters that best fit the observed light curve and then compute  $\Delta\chi^2$  between the triple and binary fits.
- (2) We repeat the above process for many different orientation angles  $\psi$  of the second planet.
- (3) The detection efficiency for a given  $(s_2, q_2)$  is estimated as the fraction of the angles  $\psi$  that produce significant deviations in the light curve. Then, the confidence level of excluding an additional planet corresponds to the efficiency.

As a criterion for planet detections, we set a threshold value  $\Delta\chi^2_{\text{th}}$ . Gould et al. (2010) suggested plausible values in the range  $\Delta\chi^2_{\text{th}} = 350 - 700$  based on their experience in fitting lensing light curves for which planets were detected through the high-magnification channel. Cassan et al. (2012) suggested a similar threshold. In our analyses, we adopt a median value  $\Delta\chi^2_{\text{th}} = 500$ .

Figure 3 shows the exclusion diagrams of the individual events. For each diagram, the regions with different confidence levels of excluding additional planets are marked in different colors. The star mark corresponds to the planet detected in the previous analysis. The upper  $x$  label represents the projected planet-host separation in a physical unit (AU). The ticks marked by “J”, “S”, “U”, and “E” represent the planet masses corresponding to the Jupiter, Saturn, Uranus, and Earth of the Solar system, respectively. We note that the conversion from  $(s_2, q_2)$  to the physical separation and mass of the planet is done based on the physical Einstein radius  $r_E$  and total mass of the lens system  $M_{\text{tot}}$  determined in the previous analyses, i.e.,  $r_{\perp} = sr_E$  and  $M_{p,2} = [q_2/(1+q_1+q_2)]M_{\text{tot}}$ .

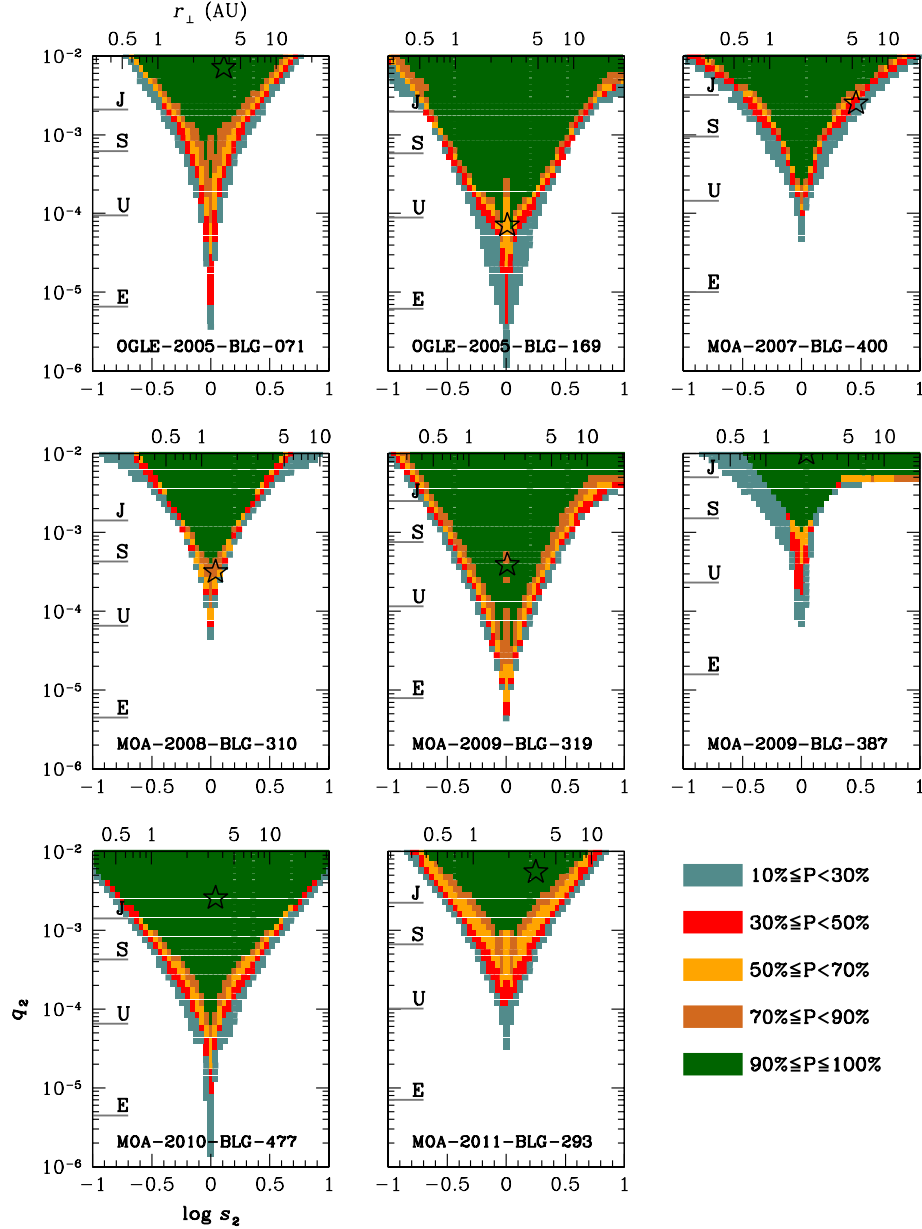


FIG. 3.— Exclusion diagrams showing the confidence levels excluding the existence of an additional planet with respect to the separation  $s_2$  and the mass ratio  $q_2$ . For each panel, the upper  $x$  label represents the planet-host separation in physical units. The ticks marked by “J”, “S”, “U”, and “E” represent the planet masses corresponding to the Jupiter, Saturn, Uranus, and Earth of the Solar system. The star marks in the individual diagrams represent the planets detected from the previous analyses.

In Table 2, we present the exclusion ranges of additional planets determined with 90% confidence level for Jupiter, Saturn, and Uranus-mass planets. It is found that the constraint on giant planets is considerably strong. On the other hand, the constraint on planets with masses less than Uranus is relatively weak. The weak constraint on low-mass planets is due to the small size of the planet-induced central caustic which decreases rapidly with the decrease of the planet mass (Chung et al. 2005). In addition to planet masses, the sensitivity depends on various other factors. Some of these factors are related to observation, including the photometric precision, cadence, and completeness of the planetary signal coverage, etc. Other factors are related to the intrinsic properties of planetary events, including the peak magnifications, severeness of finite-source effects, etc.

For OGLE-2005-BLG-169, MOA-2009-BLG-319, and MOA-2010-BLG-477, the constraint is strong. These events have a common property of high peak magnifications with  $A_{\max} = 880, 208$ , and  $599$ , respectively.

By contrast, the constraint is relatively weak for OGLE-2005-BLG-071 ( $A_{\max} = 59$ ) and MOA-2009-BLG-387 ( $A_{\max} = 49$ ) because the peak magnifications are low. For planets either with low masses or located away from the Einstein ring of the host, the central caustic is small and thus signals of low-mass planets can be detected only for very high-magnification events where the source trajectories approach close to the caustic.

For MOA-2007-BLG-400 and MOA-2008-BLG-310, the peak magnifications are high:  $A_{\max} = 629$  and  $A_{\max} = 366$ , respectively. Nevertheless, the sensitivity is relatively low. We

find the main cause of the low sensitivity for these events is severe finite-source effects, which wash out planetary signals, especially for low-mass planets (Bennett & Rhie 1996).

For MOA-2011-BLG-293, on the other hand, the sensitivity is not very high although the event was highly magnified ( $A_{\max} = 418$ ) and experienced little finite-source effects. We find that the low sensitivity is mainly due to low photometric precision caused by the source faintness.

## 5. CONCLUSION

In order to investigate the potential existence of additional planets, we reanalyzed high-magnification microlensing events for each of which a single planet had been previ-

ously detected. We found that introducing additional planets improves fits but the levels of improvement are not big enough to firmly identify additional planets. Although no clear evidence of additional planets was found, we could constrain the existence of additional planets in the parameter space. For this purpose, we presented exclusion diagrams showing the confidence levels excluding the existence of an additional planet as a function of its separation and mass ratio. We also presented the exclusion ranges of additional planets with 90% confidence level for Jupiter, Saturn, and Uranus-mass planets.

This work was supported by the research grant of Chungbuk National University in 2012.

## REFERENCES

- Albrow, M. D., Beaulieu, J.-P., Caldwell, J. A. R., et al. 2000, *ApJ*, 535, 176  
 Bachelet, E., Shin, I.-G., Han, C., et al. 2012, *ApJ*, 754, 73  
 Batista, V., Gould, A., Dieters, S., et al. 2011, *A&A*, 529, 102  
 Bennett, D. P., & Rhie, S. H. 1996, *ApJ*, 472, 660  
 Bennett, D. P., Rhie, S. H., Nikolaev, S., et al. 2010, *ApJ*, 713, 837  
 Cassan, A., Kubas, D., Beaulieu, J.-P., et al. 2012, *Nature*, 481, 167  
 Chung, S.-J., Han, C., Park, B.-G., et al. 2005, *ApJ*, 630, 535  
 D'Angelo, G., & Lubow, S. H. 2008, *ApJ*, 685, 560  
 Dong, S., DePoy, D. L., Gaudi, B. S., et al. 2006, *ApJ*, 642, 842  
 Dong, S., Bond, I. A., Gould, A., et al. 2009, *ApJ*, 698, 1826  
 Dong, S., Gould, A., Udalski, A., et al. 2009, *ApJ*, 695, 970  
 Gaudi, B. S., Naber, R. M., & Sackett, P. D. 1998, *ApJ*, 502, 33  
 Gaudi, B. S., & Sackett, P. D. 2000, *ApJ*, 528, 56  
 Gaudi, B. S., Bennett, D. P., Udalski, A., et al. 2008, *Science*, 319, 927  
 Gould, A., & Loeb, A. 1992, *ApJ*, 396, 104  
 Gould, A. 1992, *ApJ*, 392, 442  
 Gould, A., Udalski, A., An, D., et al. 2006, *ApJ*, 644, L37  
 Gould, A., Dong, S., Gaudi, B. S., et al. 2010, *ApJ*, 720, 1073  
 Gould, A., Udalski, A., Shin, I.-G., et al. 2014, *Science*, 345, 46  
 Griest, K., & Safizadeh, N. 1998, *ApJ*, 500, 37  
 Han, C., Chang, H.-Y., An, J. H., & Chang, K. 2001, *MNRAS*, 328, 986  
 Han, C. 2005, *ApJ*, 629, 1102  
 Han, C., Udalski, A., Choi, J.-Y., et al. 2013, *ApJ*, 762, L28  
 Ida, S., & Lin, D. N. C. 2004, *ApJ*, 604, 388  
 Janczak, J., Fukui, A., Dong, S., et al. 2010, *ApJ*, 711, 731  
 Kayser, R., Refsdal, S., & Stabell, R. 1986, *A&A*, 166, 36  
 Kubas, D., Cassan, A., Dominik, M., et al. 2008, *A&A*, 483, 317  
 Lissauer, J. J., Marcy, G. W., Rowe, J. F., et al. 2012, *ApJ*, 750, 112  
 Lubow, S. H., & Ida, S. 2011, *Exoplanets*, ed. S. Seager (Tucson: University of Arizona Press), 347  
 Mao, S., & Paczyński, B. 1991, *ApJ*, 374, L37  
 Mayor, M., & Queloz, D. 1995, *Nature*, 378, 355  
 Miyake, N., Sumi, T., Dong, S., et al. 2011, *ApJ*, 728, 120  
 Park, H., Udalski, A., Han, C., et al. 2013, *ApJ*, 778, 134  
 Poleski, R., Skowron, J., Udalski, A., et al. 2014, *ApJ*, 795, 42  
 Rhie, S. H. 2002, *arXiv:astro-ph/0202294*  
 Rowe, J. F., Bryson, S. T., Marcy, G. W., et al. 2014, *ApJ*, 784, 45  
 Schneider, P., & Weiss, A. 1986, *A&A*, 164, 237  
 Schneider, J., Dedieu, C., Le Sidaner, P., et al. 2011, *A&A*, 532, 79  
 Shin, I.-G., Udalski, A., Han, C., et al. 2011, *ApJ*, 735, 85  
 Shin, I.-G., Han, C., Choi, J.-Y., et al. 2012, *ApJ*, 755, 91  
 Skowron, J., Udalski, A., Gould, A., et al. 2011, *ApJ*, 738, 87  
 Song, Y.-Y., Mao, S., & An, J. H. 2014, *MNRAS*, 437, 4006  
 Udalski, A., Jaroszyński, M., Paczyński, B., et al. 2005, *ApJ*, 628, L109  
 Witt, H. J. 1990, *A&A*, 236, 311  
 Wolszczan A., & Frail, D. A. 1992, *Nature*, 355, 145  
 Yee, J. C., Shvartzvald, Y., Gal-Yam, A., et al. 2012, *ApJ*, 755, 102